

**M. A. Shehadeh<sup>1</sup>**

Department of Mechanical Engineering,  
American University of Beirut,  
Beirut 1107 2020, Lebanon  
e-mail: ms144@aub.edu.lb

**P. El Ters**

Department of Mechanical Engineering,  
American University of Beirut,  
Beirut 1107 2020, Lebanon  
e-mail: pme00@mail.aub.edu

**R. W. Armstrong**

Department of Mechanical Engineering,  
University of Maryland,  
College Park, MD 20742  
e-mail: rona@umd.edu

**W. Arnold**

MBDA-TDW,  
Schrobenhausen 86523, Germany  
e-mail: werner.arnold1@gmx.net

# Dislocation Mechanics of Extremely High Rate Deformations in Iron and Tantalum

*High strain rate simulations were performed using the multiscale dislocation dynamic plasticity (MDDP) method to calculate different rise times and load durations in mimicking high deformation rate shock or isentropic (ramp) testing of  $\alpha$ -iron and tantalum crystals. The focus for both types of loading on both materials was on the inter-relationship between the (dislocation-velocity-related) strain rate sensitivity and the (time-dependent) evolution of dislocation density. The computations are compared with model thermal activation strain rate analysis (TASRA), phonon drag, and dislocation-generation predictions. The overall comparison of simulated tests and previous experimental measurements shows that the imposition of a rise time even as small as 0.2 ns preceding plastic relaxation via the MDDP method is indicative of relatively weak shock behavior.*

[DOI: 10.1115/1.4052104]

*Keywords:* constitutive relations, mechanical behavior, microstructure property relationships

## Introduction

Inelastic deformation in crystalline metals results from the generation and motion of dislocations: line defects that sweep across the crystal slip planes when the applied mechanical stress is high enough to overcome a generally complicated lattice resistance. Most real materials contain a large number of dislocations whose collective behavior, when activated, produces complex interactions between themselves and electrons, phonons, and other defects to control plastic yielding, strain hardening, and subsequent material fracturing.

Under extreme thermo-mechanical loadings such as shock compression or somewhat more gradual ramp-type high strain rate deformation, the dislocation responses are predicted to differ significantly for the two types of loading and to differ also from the behaviors at lower strain rates [1–4]. It is widely believed that under extremely high loading rates, the dislocation motion changes from a thermally activated mechanism to a uniform drag-controlled resistance. For example, both shock and isentropic (ramp) compression investigations of (bcc) ARMCO iron and tantalum as well as of (fcc) copper and aluminum materials have established strong increases in measured strength levels [1,5–10]. In a work by Smith et al. [1] involving ramp-type compression tests of aluminum and  $\alpha$ -iron, a transition from a logarithmic dependence of yield stress on strain rate to a stronger power-law dependence was reported. Eggert et al. [9] performed ramp compression experiments on tantalum at different strain rates and reported a transition at  $10^5 \text{ s}^{-1}$  to a higher rate dependence that was attributed to a changeover from a thermally activated dislocation mechanism to a drag-controlled one. Asay et al. [10] showed that the mechanical response of tantalum similarly changed at  $\sim 10^6 \text{ s}^{-1}$ . Zaretsky and Kanel [4] reported further that beyond the phonon drag mechanism operative at higher strain rates, an increase in dislocation multiplication also entered to strongly influence deformation behavior.

Atomistic simulations carried out by Zepeda-Ruiz et al. [11] on ramp compression of tantalum showed that deformation twinning became rate-controlling over slip behavior under very high strain rate conditions. A compressive stress for single crystal deformation twinning of 8.0 GPa was reported as compared with a previously listed value [6] of  $\sim 0.8$  GPa reported for bulk polycrystalline material. Grain-size-dependent deformation twinning was also shown to occur near the slip-induced yield stress level of shocked polycrystalline  $\alpha$ -iron material [12]. Armstrong, Arnold, and Zerilli (AAZ) reported alternative dislocation model descriptions differentiating between the deformation behavior of metals under conventional and shock versus quasi-isentropic (ramp-type) *shockless* loading [6,12]. At relatively low (conventional) strain rates,  $\dot{\epsilon}$ , in compression, the occurrence of thermally activated slip was proposed to follow the widely employed Orowan relation [13]

$$\dot{\epsilon} = \frac{1}{m} \rho b v \quad (1)$$

in which  $m$  is a polycrystalline Taylor-type orientation factor,  $\rho$  is an essentially constant dislocation density,  $b$  is the dislocation Burgers vector, and  $v$  is the dislocation velocity that is controlled by thermal-overcoming of interrupted “stops” along the crystal slip plane. On this basis, the dependence of flow stress on strain rate was taken to follow a model thermal activation strain rate analysis (TASRA) relationship that had been proposed for slip of bcc metals by Zerilli and Armstrong (Z–A) in the form [14]

$$\sigma = \sigma_G + B_0 [\exp(-\beta_0 T)] \left( \frac{d\epsilon}{dt} \right)^{\frac{kT}{W_0}} + k_\epsilon l^{-1/2} \quad (2)$$

where  $\sigma$  is the unidirectional compressive stress (equal to  $\sqrt{3}$  times the von Mises equivalent stress,  $\sigma_{vM}$ ) and is related to the applied shear stress,  $\tau$ , through the same Taylor factor  $m$  in  $\sigma = m\tau$ ;  $\epsilon$  is the compressive strain;  $\sigma_G$  is an athermal stress;  $k$  is Boltzmann’s constant,  $T$  is the absolute temperature;  $k_\epsilon$  is the Hall–Petch stress intensity;  $l$  is the average polycrystal grain diameter; and  $B_0$ ,  $\beta_0$ , and  $W_0$  are experimental constants. The experimental constants had been determined for both  $\alpha$ -iron [14] and tantalum [15] materials.

<sup>1</sup>Corresponding author.

Contributed by the Materials Division of ASME for publication in the JOURNAL OF ENGINEERING MATERIALS AND TECHNOLOGY. Manuscript received December 22, 2020; final manuscript received April 16, 2021; published online September 3, 2021. Assoc. Editor: Tariq Khraishi.

Under shock compression, however, the AAZ model description was proposed to changeover from thermally activated slip to dislocation generation at the shock front [6]. Such dislocation generation would occur homogeneously or by sudden multiplication from the initially resident dislocation density [6,7] in accordance with a limiting dislocation rate equation that had been proposed by Orowan [8,12]

$$\frac{dy}{dt} = \left( \frac{d\rho}{dt} \right) b \Delta x \quad (3)$$

in which  $dy/dt$  is the plastic shear strain rate,  $d\rho/dt$  is the rate of dislocation generation, and  $\Delta x$  is a characteristic dislocation displacement for the generated dislocations. The need for significant dislocation generation becomes important for shock loading, in principle, because the large value of induced shear strains at all nanometer-scale points along a propagating shock front are not able to be relieved by the relatively remote displacement of micrometer- or larger-scale separations normally applicable for resident dislocation densities [6]. This limiting condition was also specified on a TASRA basis in terms of a smallest constant activation volume being achieved for the mechanism in which case, the effective compressive stress was obtained as [15]

$$\sigma = \frac{2U_0}{v_0} - \frac{2kT}{v_0} \ln \left[ \frac{(d\varepsilon/dt)_0}{(d\varepsilon/dt)} \right] \quad (4)$$

Figure 1 illustrates the behavioral transition for very recently reported [16] split Hopkinson pressure bar (SHPB) measurements made on copper material, with and without stress interruption, in comparison with a previous compilation [6,12] of conventional, SHPB, and shock results. The lower, approximately linear, stress dependencies, at two strain values, apply for Eq. (2) behavior and the more steeply-rising dashed curve that had been determined by Swegle and Grady [17] for higher shock measurements were shown also to follow the linear double-line dependence that is shown in the figure to apply for Eq. (4) behavior.

A similar upturn at somewhat lower strength levels, say, appearing at  $\geq 10^4 \text{ s}^{-1}$  for isentropic shockless compression is believed to be caused, at least initially, by the motion of a normally resident dislocation density whose limiting high-speed motion might be so high as to be only retarded by the mechanism of phonon drag [1], thus highlighting the importance of the resident dislocation density in determining the initial level of the material flow stress. In the case of drag-determined stress, direct linear dependence of  $\sigma$  on  $(d\varepsilon/dt)$  would be expected, as reported for stress levels exceeding  $\sim 7 \text{ GPa}$  for copper [12,18].

Somewhat surprisingly, recent dislocation dynamics simulations performed by El Ters and Shehadeh [19] have shown that the yield stresses accompanying shock and ramp compression are much closer than those shown in the previously described experiments. Ramp and shock compressions are both fundamental problems of

microscopic plasticity involving wave-dislocation interactions which fall within the realm of the discrete dislocation dynamics (DDD) method. In the past three decades, DDD has been extensively used to address several aspects of metal plasticity, especially some of which come under extremely high strain rate shock compression. For example, shock-induced plasticity in fcc metals has been investigated using the multiscale dislocation dynamics plasticity (MDDP) framework; the results were used to develop physics-based models capable of predicting material behaviors under such violent conditions. Thus, the capabilities of MDDP have been applied to evaluate shock and ramp compression in bcc metals [3,19]. In the present article, we report more details on the MDDP method of assessing the initial rise times, strain rate sensitivity, and dislocation evolution dependencies of flow stress calculations for both shock and ramp compression of bcc  $\alpha$ -iron and tantalum crystals. The time dependence of both dislocation motion and generation is tracked in the MDDP simulations. Comparisons are made with previously reported experimental measurements and, especially, with the mentioned previously-established dislocation-based constitutive relations. Particular emphasis is given to the effect of shock rise times as compared with ramp-loading on inducing plastic yielding and follow-on deformations at higher applied rates.

## Methodology

Multiscale dislocation dynamics plasticity [20] is a hybrid elastoviscoplastic model that accounts for time-dependent plasticity through the explicit three-dimensional (3D) evaluation of dislocation nucleation, generation, and motion. MDDP is a simulation model that couples the 3D discrete dislocation dynamics with finite element (FE) analysis [21,22].

At the macro-level, the mass, momentum, and energy transport obey the basic laws of continuum mechanics, i.e., the linear momentum and the energy balance equations are applied by assuming that 90% of the work is transformed into heat such that

$$\text{div } S = \hat{\rho} \dot{v}_p \quad (5)$$

$$\hat{\rho} C_v \dot{T} = 0.9 S \dot{\varepsilon}^p \quad (6)$$

where  $S$  is the Cauchy stress tensor,  $\hat{\rho}$  is the density,  $v_p$  is the particle velocity, and  $C_v$  is the specific heat. As mentioned previously, since the behavior is elastoviscoplastic, the strain rate  $\dot{\varepsilon}$  is decomposed into an elastic part  $\dot{\varepsilon}^e$  and a plastic part  $\dot{\varepsilon}^p$

$$\dot{\varepsilon} = \dot{\varepsilon}^e + \dot{\varepsilon}^p \quad (7)$$

The mechanical response is then calculated by assuming the incremental form of Hooke's law such that

$$\hat{\sigma} = [C^e][\dot{\varepsilon} - \dot{\varepsilon}^p] \quad (8)$$

in which  $\hat{\sigma}$  is the co-rotational stress rate and  $C^e$  is the generalized anisotropic stiffness tensor that depends on the pressure, temperature, and crystal orientation.

In the discrete dislocation dynamics part of the code, plasticity is obtained by the analysis of the dislocations history evolution. Dislocation curves are discretized into small segments of mixed character. These segments move according to the Newtonian equation of motion such that [23,24]:

$$F_{P-K} = d(T, v, \theta) v + m_e \dot{v} \quad (9)$$

where  $F_{P-K}$  is the Peach Koehler force,  $m_e$  is the effective mass of the moving dislocations [25],  $v$  is the dislocation velocity, and  $d$  is the dislocation drag coefficient, which is a function of temperature  $T$ , velocity  $v$  and the dislocation character  $\theta$  (i.e., the angle between the dislocation line sense and its Burgers vector) [26–29].

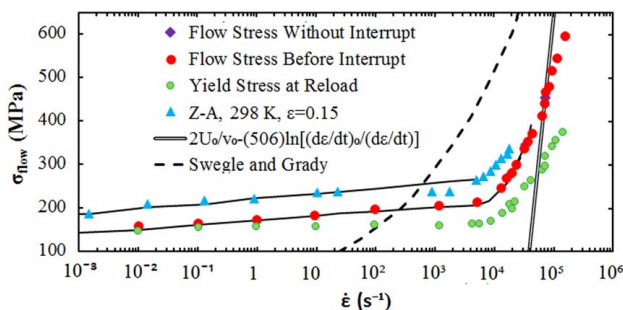


**Fig. 1** A compilation [6,12,16] of copper conventional and split Hopkinson pressure bar measurements leading at higher pressures to two stress dependencies [15,17] proposed to be applicable for shock-induced strength behaviors.

The mobility equation adopted in MDDP is as follows:

$$d(T, v, \theta) = \frac{d_0}{1 - \left(\frac{v}{c_t}\right)^2} \times \frac{T}{T_{cr}} \quad (10)$$

where  $T_{cr}$  is the critical temperature of the material which is the temperature above which the mobility of screw dislocation equalizes that of an edge dislocation;  $d_0$  is the dislocation drag at the reference temperature, and  $v$  is the glide velocity.

The Peach–Koehler force is computed numerically at each time-step as described in Zbib et al. [25]

$$F_{P-K} = F_{friction}(\sigma_P, T) + F_D + F_{self} + F_{external} + F_{obstacle} + F_{image} \quad (11)$$

In Eq. (11),  $F_{friction}$  is the friction force associated with the Peierls potential,  $F_D$  is the dislocation–dislocation interaction force,  $F_{self}$  is the self-force,  $F_{external}$  is the externally applied loads,  $F_{obstacle}$  is the dislocation-obstacle force, and  $F_{image}$  is the image force.

The above-mentioned equations are solved to obtain the nodal values of the dislocation segment velocity and positions. The plastic strain rate is computed as follows:

$$\dot{\epsilon}^p = \sum_{i=1}^N \frac{l_i v_{gi}}{2V} (n_i \otimes b_i + b_i \otimes n_i) \quad (12)$$

where  $l_i$  is the segment dislocation length,  $n_i$  is the unit vector normal to the slip plane, and  $V$  is the representative volume element.

The momentum equation is then solved numerically using explicit forward integration [20]

$$[M]\{\ddot{U}\} + [C]\{\dot{U}\} + [K]\{U\} = \{f\} \quad (13)$$

where  $[M]$  is the mass matrix,  $[C]$  is the damping matrix,  $[K]$  is the stiffness matrix,  $\{U\}$  is the nodal displacement, and  $\{f\}$  is the force vector. At each time-step, the stiffness matrix is adjusted to account for the elastic constant dependence on the pressure as shown in Table 1.

A noteworthy feature of the model is the incorporation of a strain rate and temperature-dependent mobility law based on atomistic calculations as discussed in Refs. [3,19,24,35]. Previous MDDP simulations [3,19,22,36–40] investigated the wave-dislocations interactions under shock and ramp compression in single crystals. Shock and ramp loadings result in nonlinear elastic behavior which is accounted for in the finite element part of the code by the pressure dependence of the elastic constants as described previously [19] and summarized in Table 1.

The information in Table 1 is employed in the present report to mimic ramp compression in bcc  $\alpha$ -iron and tantalum single crystals. The samples are oriented in the [001] direction that is aligned with the ramp wavefront propagation direction. The ramp wave is generated by applying a velocity-controlled boundary condition at the upper surface of the sample in the  $z$ -direction. Ramp wave loading involves uniaxial strain compression where the four sides

**Table 1 Mechanical properties of  $\alpha$ -iron [30–32] and tantalum [33,34] single crystals at 300 K**

Temperature (K)	$\alpha$ -iron	Tantalum
Burgers vector $b$ (nm)	0.248	0.286
Density $\hat{\rho}$ (kg m <sup>-3</sup> )	7860	16595
Poisson ratio $\nu$	0.37	0.34
$C_{11}$ (Pa)	$5.1831P + 2.87 \times 10^{11}$	$3.7613P + 3 \times 10^{11}$
$C_{12}$ (Pa)	$4.11P + 1.96 \times 10^{11}$	$2.2385P + 2 \times 10^{11}$
$C_{44}$ (Pa)	$2.6179P + 9.102 \times 10^{10}$	$0.9888P + 5 \times 10^{10}$

Note:  $P$  in the elastic constant equations is the applied pressure in Pa. It is equal to the unidirectional compressive stress  $\sigma$ .

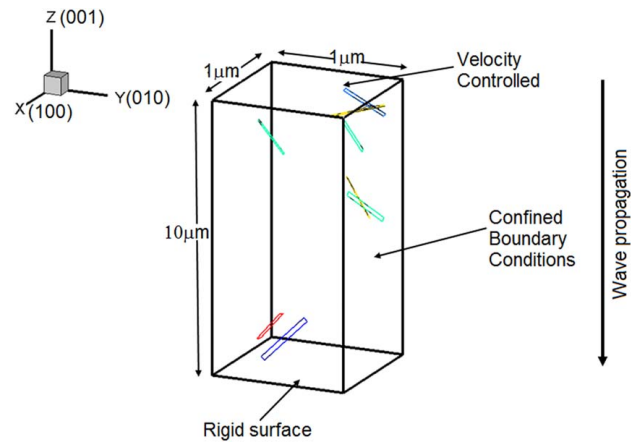


**Fig. 2 Simulation setup for a dimensional  $1 \times 1 \times 10 \mu\text{m}$  sample. The colored line segments represent potential Frank Read source lengths for dislocation generation. The stress wave is created by imposing a controlled-velocity to the top surface. The particle velocity increases linearly up to a specified rise time after which the velocity is held constant.**

of the  $l_i$  domain are confined while the lower surface is rigidly fixed as illustrated in Fig. 2. The strain rate is calculated by taking the derivative of the plastic strain in each finite element cell with respect to time where the stress and strain tensors are computed at each simulation time-step in the finite element part of the code. In all of the below simulations, an initial dislocation density of  $10^{13} \text{ m}^{-2}$  was used. Frank read (FR) sources of  $0.35 \mu\text{m}$  to  $0.5 \mu\text{m}$  length were randomly introduced in the simulated domain to act as agents for dislocation generation and multiplication. The material properties used for the  $\alpha$ -iron and tantalum samples are summarized in Table 1.

## Results and Discussion

Multiscale dislocation dynamics plasticity simulations were performed to mimic the induced plasticity under ramp compression of  $10\text{-}\mu\text{m}$  thickness  $\alpha$ -iron and tantalum single crystals oriented in the [001] direction. The rise time of the compressive waves was investigated for steeper shock waves (0.2 ns and 1.0 ns) versus slower ones (5.0 ns) and also to be compared with longer ramp loading in compression (20 ns and 40 ns). All of the MDDP results were computed as average values over the upper quarter of the simulation sample that is illustrated in Fig. 2. We are calculating the results over the upper quarter of the simulation because our intention is not to calculate the peak pressure but rather to find the instant the yielding is taking place, i.e., the stress required to activate a dislocation in order to study the effect of rise time.

The computed MDDP von Mises stress histories at different rise times are plotted in Fig. 3(a) for  $\alpha$ -iron and Fig. 3(b) for tantalum, in both cases at an effective plastic strain rate of  $10^7 \text{ s}^{-1}$  and with  $\sigma_{vM} = \sigma/\sqrt{3}$ . The responses for both materials are generally similar but showing different quantitative behaviors for comparable rise times. At 0.2-ns and 1.0-ns rise times, the two shocked crystals exhibit abrupt elastic overshoot taking place behind the shock fronts, then to be followed by fast plastic relaxation. For an intermediate 5-ns rise time and for the longer ramp loadings of 20 ns and 40 ns, the elastic overshoot is still apparent but the process of plastic relaxation takes place at the ramp front well before the peak pressure is attained. As the rise time increases, the peak value of the stress decreases and a more gradual stress relaxation is manifested. This stress relaxation is the result of dislocation interaction with the wavefront. For the shock cases and short ramping rise times, the maximum velocity of the wave is quickly reached and the shear stress increases rapidly. As a result, the shear stress

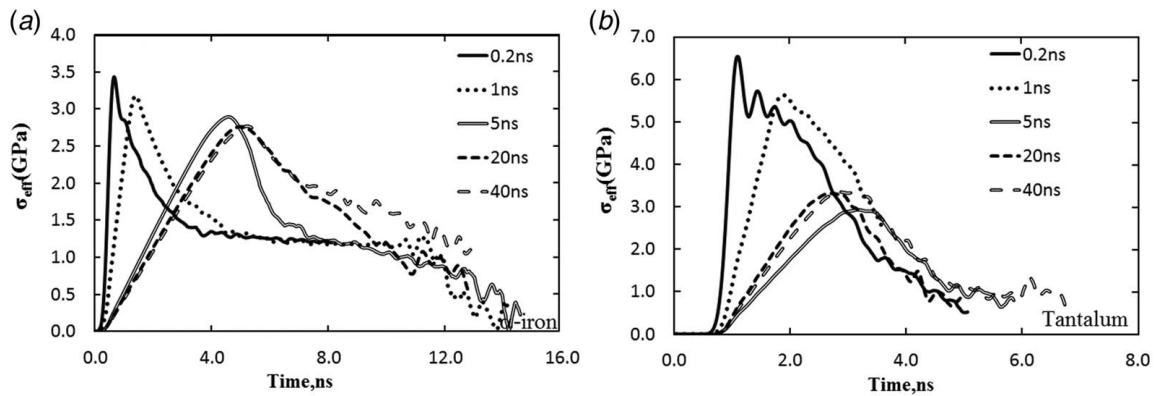


**Fig. 3** Effective von Mises stress histories at different rise times for (a)  $\alpha$ -iron and (b) tantalum crystals subjected to a compressive plastic strain rate of  $10^7 \text{ s}^{-1}$

overcomes the lattice friction within a very short period of time, leading to rapidly induced plasticity and consequently rapid stress relaxation. For the longer ramp rise times, the wavefront gradually builds up such that the dislocations have ample time to cause relaxation at the ramp front.

**Operative Stress Levels.** The stresses for onset of initial yielding for the  $\alpha$ -iron and tantalum crystals, expressed as von Mises stresses,  $\sigma_{vM}$ , are plotted against the same type von Mises plastic strain rate in Fig. 4. Several previously reported results are also shown [9,10,41]. The figure shows that the current yield stress measurements are sensitively dependent on the rise time in both shock and ramp compression loading such that higher yield stress obtains for a shorter rise time. Yielding under the longer time ramp loading is relatively less sensitive to the rise time. Very importantly, the yield stress is shown to increase strongly with an increase in the plastic strain rate, more so than the behavior exhibited in lower imposed strain rate tests [14]. The rise in the strain-rate-dependent stress is greater at shorter rise times. Higher strain rates than predicted by the constitutive model of Eggert et al. [9] as well as by the referenced experimental measurements [10,41] are shown to have been achieved.

**Strain Rate Sensitivity.** The strain rate-dependent yield stresses shown in Fig. 4 are able to be further assessed via the AAZ description of the TASRA [14,42]. Figures 5(a) and 5(b) show the addition of the MDDP calculations to a number of the previously compiled measurements described, respectively, for  $\alpha$ -iron [6,8,42] and

tantalum [6,7] materials. Starting in the low-stress region of Fig. 5(a), there is excellent agreement between the isentropic MDDP  $\alpha$ -iron results and the Z-A solid line for TASRA-based slip running across the bottom of the figure. At a stress level of  $\sim 1.0$  GPa, the Z-A line for slip behavior was shown to be competitive with the bulk deformation twinning stress for the same material [6,12]. Likewise, the open-diamond points computed separately for “MDDP Shock Yield” are near to the somewhat higher open triangle “Arnold Yield” points [6,42]. The dash-dot line for limiting “AAZ Slip” behavior was predicted for a smallest possible strain rate sensitivity determined activation volume  $v^*$  value for slip [6,13] (soon to be described) and the predicted line may be seen to connect with correspondingly computed “MDDP Shock Flow”

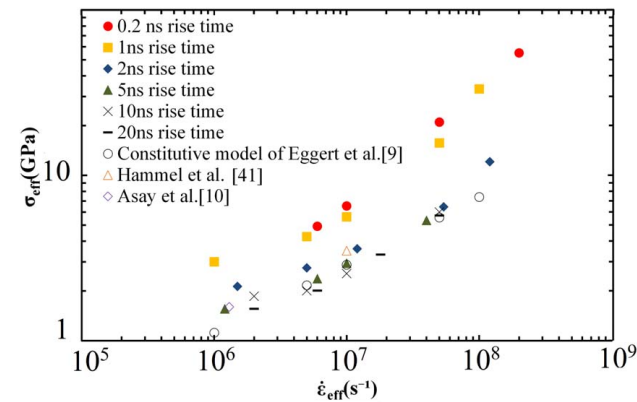


**Fig. 4** Tantalum effective von Mises yield strength versus effective von Mises plastic strain rates at different rise times. The yield strength is seen to increase strongly with an increase in the plastic strain rate [14].

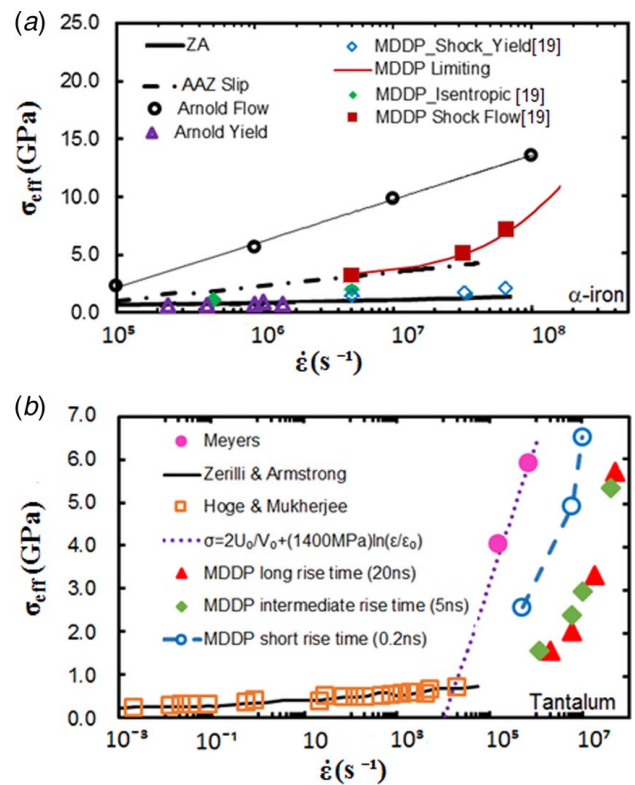


**Fig. 5** Comparison of results: (a) for  $\alpha$ -iron, of Armstrong, Arnold, and Zerilli TASRA model [6] and MDDP calculations of El Ters and Shehadeh [19] and (b) for tantalum, of the present MDDP-generated results and the TASRA model proposed by Armstrong, Arnold, and Zerilli [12].

filled-square stresses and the “MDDP Limiting” curve dependence from El Ters and Shehadeh [19]. Other stress dependencies described in Ref. [8] have been shown to be shifted to even higher strain rates, including the important measurements of Smith et al. [1]. The highest open-circle points in Fig. 5(a) are the “Arnold Flow” stress measurements [42] that were accounted for by nano-scale deformation twinning according to Eq. (4) [6,12]. Thus, the total comparison of  $\alpha$ -iron measurements and MDDP computations in Fig. 5(a) are in reasonable agreement with the previous TASRA-based slip and twinning descriptions but fall significantly short of reaching Arnold’s shock measurements attributed to nano-scale twinning.

The MDDP calculations for tantalum follow a similar trend to those of  $\alpha$ -iron as shown more clearly in Fig. 5(b). In this case, the lower solid line for the Z–A description follows closely the TASRA-based description of experimental measurements, and here also, the steeper dotted line through the filled-circle experimental flyer-plate shock measurements [6] was attributed on a limiting small activation volume basis to stress-control by nano-scale deformation twinning. The measured shock stresses in Fig. 5(b) are lower than the 8.0 GPa deformation twinning stress reported by Zepeda-Ruiz et al. [11] but not appreciably so. Other SHPB measurements on tantalum had been shown to increase towards the steeper shock dependence in the same manner as shown for copper in Fig. 1 [7]. In Fig. 5(b), the MDDP-generated stresses for both shock and isentropic compression are seen also to fall significantly below the experimental shock measurements, more so at longer rise times. Additional insight into the measurements is provided on the basis of corresponding activation volume calculations derived from a TASRA description of the strain rate-dependent flow stress values shown in Fig. 4.

**The Thermal-Stress-Associated Activation Volume.** The strain rate sensitivity of the MDDP results is assessed in terms of the TASRA-based activation volume parameter that is computed, for example, from the equation [43–45]

$$v^* = mkT \left[ \frac{\partial \ln(\dot{\epsilon})}{\partial \sigma} \right]_T \quad (14)$$

In Eq. (14),  $v^*$  is an activation volume that is equal to an activation area,  $A^*$ , times the dislocation Burgers vector,  $b$ ;  $m$  is a Taylor polycrystal orientation factor that is replaced by the reciprocal Schmid factor, 2.45, for the [001] crystal orientation in Fig. 2; Boltzmann’s constant,  $k = 1.38 \times 10^{-23}$  J/K;  $\dot{\epsilon}$  is the von Mises plastic strain rate; and  $\sigma$  is the compressive stress,  $\sigma = (\sqrt{3}) \sigma_{VM}$ . The activation volume,  $v^*$ , has been found to be proportional to the reciprocal value of the thermal stress,  $\tau_{Th}$ , for the strain rate dependence of a wide variety of metals and, very importantly, for their operative thermally activated dislocation mechanisms [14,43]. Figure 4 provided for such  $v^*$  values to be calculated between adjacent points of the various sequences of stresses over the full range of strain rates and rise times for the simulated and referenced measurements. The computations are plotted against the inverse of the thermal shear stresses taken as  $\sqrt{3}(\sigma_{VM}/2.45)$  in Fig. 6, thus building onto a previous compilation of results reported by Armstrong and Li [8]. The linear dependence in the figure is the straight-line fit made to an earlier compilation of measurements described in Ref. [45]. The reciprocal thermal shear stress,  $(\tau_{Th})^{-1}$ , on the abscissa scale in Fig. 6 is normally taken to follow the relationship

$$\tau = \tau_{Th} + \tau_G \quad (15)$$

in which  $\tau$  is the applied shear stress,  $\tau_{Th}$  is the thermal shear stress, and  $\tau_G$  is the athermal shear stress component that is only dependent on temperature,  $T$ , as the shear modulus. The athermal shear stress is determined as the stress corresponding to  $\dot{\epsilon} = 0$  [43] and is taken to be negligible for the present results. The averaged thermal shear stress for adjacent points in Fig. 4 is employed as  $\tau_{Th} = (1/2) [(\sqrt{3}) \{\sigma_{VM1} + \sigma_{VM2}\}/2.45]$ .

As depicted in Fig. 6, the computed MDDP data for  $\alpha$ -iron and tantalum, as well as the newly added results of Zepeda-Ruiz et al. [11], fit reasonably well (though a bit lower for the shorter MDDP rise times) to the higher strain rate region of the extended  $v^* - (\tau_{Th})^{-1}$  plot compiled by Armstrong and Li [8] to include other shock measurements. In this regard, it is mentioned again that the steep linear dash-dot dependence of the “AAZ Slip” line in Fig. 5 applies for a limiting small activation area for slip, that is,  $A^* = v^*/b = b^2$ , and the steeper line fitted to the “Arnold Flow” measurements corresponds to a smaller  $v^*$  value proposed to correspond to nano-scale deformation twinning with  $b_T = (1/3)$  of the  $b = (a/2) \langle 111 \rangle$  for slip [6,12]. The somewhat lower MDDP-described shock compression points in Fig. 6 for shorter rise times are consistent with Fig. 5 indication of relatively weaker shock behavior being obtained as compared with the experimental measurements. The results invite comparison with the separately MDDP-monitored dislocation density behaviors depicted in Fig. 7.

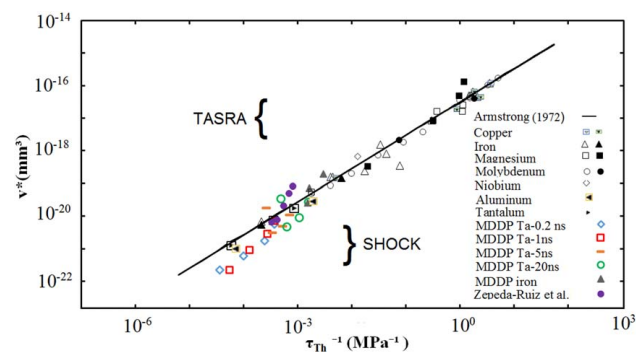


**Fig. 6 Comparison of the activation volume and thermal stress plot of Armstrong and Li [8] with MDDP tantalum and  $\alpha$ -iron computations at different rise times and with computations from the atomistic data reported by Zepeda-Ruiz et al. [11].**

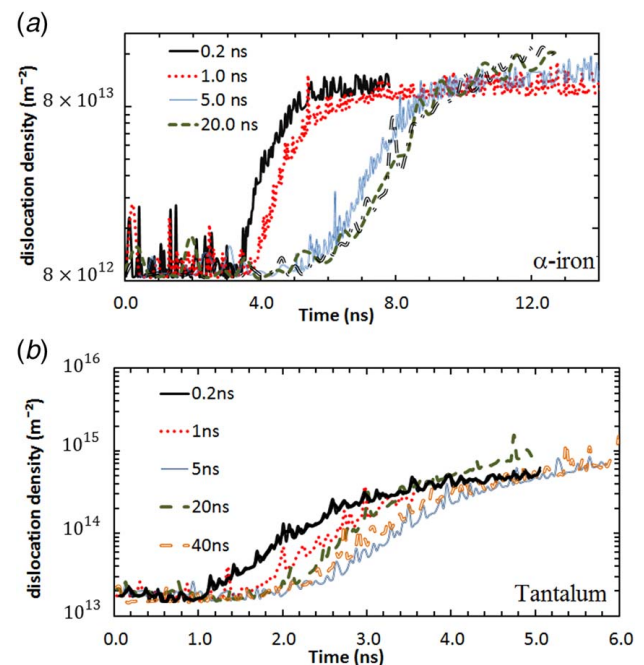


**Fig. 7 Evolution of the dislocation density at different rise times for (a)  $\alpha$ -iron and (b) tantalum**

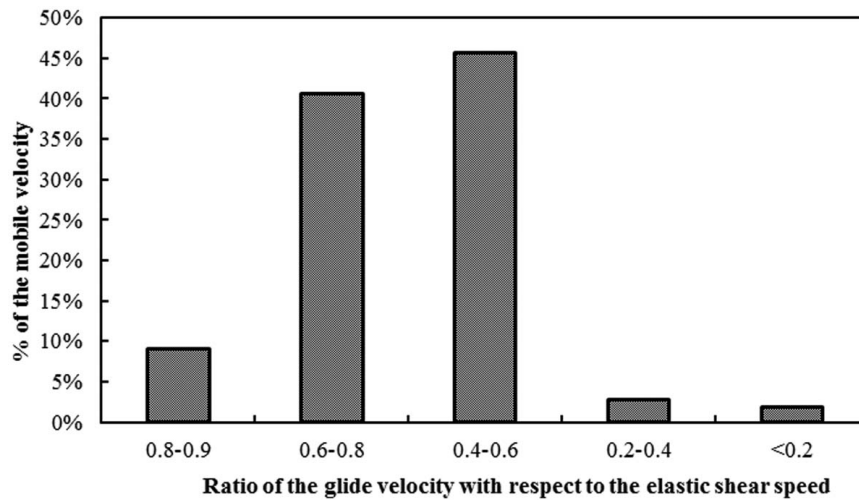


**Fig. 8** Distribution of glide velocities for the tantalum crystal relative to the elastic shear speed at 1.5 ns after a rise time of 0.2 ns for an imposed strain rate of  $5 \times 10^7 \text{ s}^{-1}$

**Dislocation Densities.** The dislocation density evolutions for different rise times in the simulated MDDP descriptions are shown for the  $\alpha$ -iron and tantalum crystals in Figs. 7(a) and 7(b). In each case, an initial dislocation density is seen to increase on the arrival of the wavefront, more strongly at shorter rise time. As the shear stress rises, the distributed dislocation sources indicated in Fig. 2 are activated and the dislocation density increases in an S-type manner. The evolved dislocation structure was reported previously to consist predominantly of elongated screw-type dislocations [19]. The edge-type dislocations were found to readily move through the crystal in accordance with other reported results [3,19,46]. The increasingly sudden yield point behavior seen at the several peak stress values exhibited in Fig. 3 resulted mainly from the motion of those screw lines. A greater rate of multiplication is naturally shown to have occurred for a faster rise time but even for the 0.2-ns result, there is not an impression of the type of discontinuous shock-front behavior expected for ideal

conditions. Quite interestingly, it might be noted that the terminal dislocation density is greater for a longer rise time including those times for ramp compression. The behavior may be seen to be linked in Fig. 3 to a more gradual stress relaxation occurring at the longer initial rise times, thus being attributed to a longer time for dislocations to interact with the traveling wavefront. From the comparison of the results in Figs. 3 and 7, it may be seen that the level of stress available to drive the same dislocation density generally is higher for the longer ramp waves. On such basis, therefore, the ramped dislocations are accelerated to average speeds higher than those under shock compression and a higher level of dislocation drag might be thought to be applicable to the present measurements as previously described for the comparative nature of ramp and shock compressions [12,18].

A histogram of dislocation slip velocities is shown in Fig. 8 for the tantalum crystal results as monitored at 1.5 ns after a 0.2-ns

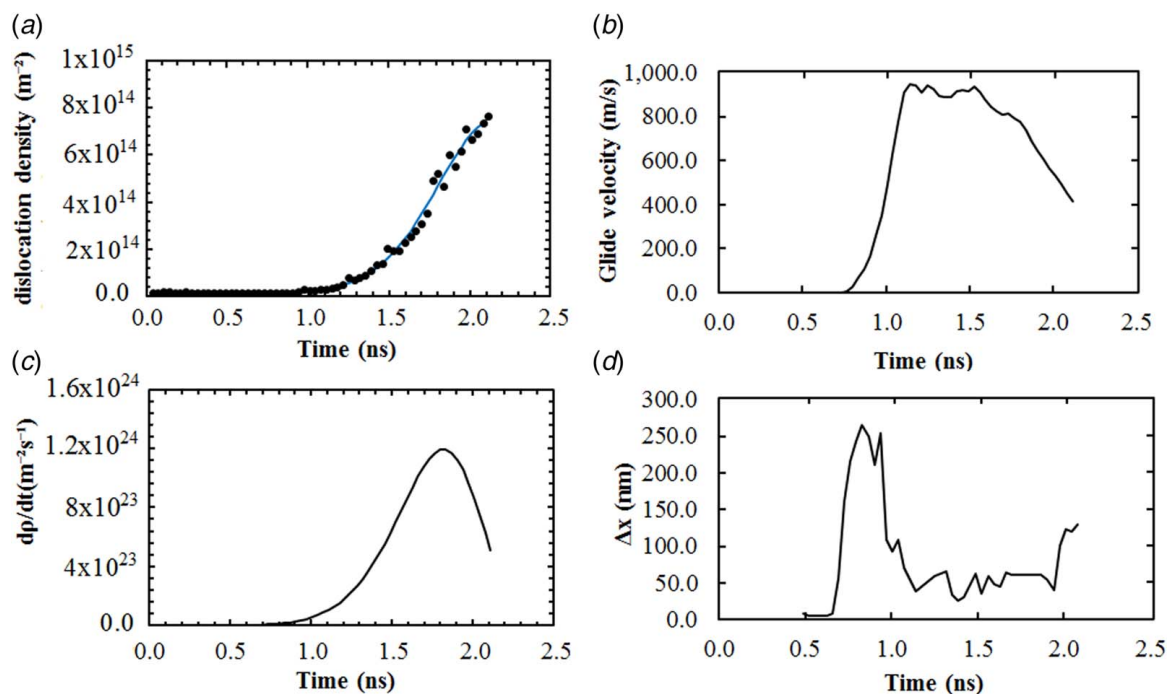


**Fig. 9** Time history of a compressed tantalum crystal at 0.2-ns rise time and  $5 \times 10^7 \text{ s}^{-1}$  plastic strain rate: (a) dislocation density, (b) glide velocity, (c) dislocation-generation rate, and (d) average dislocation displacement

rise time for an effective plastic strain rate of  $5 \times 10^7 \text{ s}^{-1}$ . Almost 10% of the dislocations are found to be moving at the speed of  $\sim 1650 \text{ m/s}$ , exceeding 80% of the shear wave velocity. A relatively high 85% of the dislocations are shown to be moving at a speed greater than  $\sim 825 \text{ m/s}$ , exceeding  $0.4 \times$  the elastic shear wave speed.

However, the dislocation travel between thermal obstacles is normally neglected in the thermal activation description. Otherwise, the presence of a significant dislocation drag would lead to a direct dependence of the stress on the plastic strain rate [7], as shown not to be the case in Figs. 5(a) and 5(b).

The relative contributions of the initial resident dislocation density and shock-generated density for the tantalum crystal may be assessed further on the basis of the generalized Orowan equation previously applied to other tantalum single crystal and polycrystal measurements [7]

$$\dot{\epsilon} = \frac{1}{m} (\rho_m b v + \dot{\rho} b \Delta x) \quad (16)$$

In Eq. (16),  $\rho_m$  is taken here as the mobile dislocation density,  $b$  is  $2.86 \times 10^{-10} \text{ m}$ ,  $v$  is the average mobile glide velocity,  $\dot{\rho}$  is the dislocation-generation rate taken from the time derivative of the dislocation density evolution, and  $\Delta x$  is to be determined as the average dislocation displacement associated with the newly generated dislocations.

The results in Fig. 8 and the parameters in Eq. (16) relate to the sequence of results shown in Figs. 9(a)–9(d) for the particular test for tantalum involving a rise time of 0.2 ns and plastic strain rate of  $5 \times 10^7 \text{ s}^{-1}$ . Figure 9(a) traces the evolution of the dislocation density. Figure 9(b) traces the dislocation glide velocity and reveals that, at  $\sim 1.1 \text{ ns}$ , a relatively constant velocity is obtained and thereafter decreases so that, as indicated in Fig. 9(a), the imposed plastic strain rate was largely determined by an increase in the dislocation density. The time dependence of the dislocation density evolution in Fig. 9(c) shows that the rate of buildup of the dislocation density increased until  $\sim 1.8 \text{ ns}$ , well-after the  $\sim 1.0\text{-ns}$  time, when the average dislocation displacement in Fig. 9(d) had fallen to a level of  $\sim 50\text{-nm}$  displacement. Thus, the initial sudden rise of the dislocation velocity to a relatively constant value of  $\sim 950 \text{ m/s}$  for more than the  $\sim 85\%$  of the fast-moving dislocations monitored in Fig. 7 is halted by the more gradual increase in dislocation generation shown in Fig. 9(c).

The post 1.0 ns, relatively large, displacement,  $\Delta x$ , in Fig. 9(d) for the generated dislocations implies that such generation has occurred away from the shock front, thus, also being in agreement with the conclusion drawn thus far that the MDDP simulation, even at the smallest rise time, is approximating a relatively weak shock condition. The result is further supported by the observation that the peak pressure reached in the currently described test of 30 GPa compares with a greater threshold stress for homogeneous dislocation nucleation being estimated for tantalum to be 65 GPa [47,48].

## Summary

The MDDP method has been employed to simulate the plasticity of  $\alpha$ -iron and tantalum materials subjected to high rate shock or isentropic loading. The focus for various shock and ramp-type loading conditions for both materials has been on TASRA and phonon drag issues associated with the several topics of initial rise times for plastic deformation; the corresponding strain rate sensitivity properties; and the evolution of dislocation densities. A comparison of the results has been made with compilations of experimental and model descriptions previously reported for the expected dislocation behaviors. Smaller differences than expected were obtained between the shock as compared to slower isentropic (ramp) loading and attributed to the shock loading being relatively weak.

## Acknowledgment

The support from the Research Board at the American University of Beirut is greatly acknowledged. This paper is dedicated to the memory of our beloved colleague and friend Hussein M. Zbib who passed away on February 10, 2020.

## Conflict of Interest

There are no conflicts of interest.

## Data Availability Statement

The data sets generated and supporting the findings of this article are obtainable from the corresponding author upon reasonable request. The authors attest that all data for this study are included in the paper. Data provided by a third party are listed in Acknowledgment. No data, models, or code were generated or used for this paper.

## References

- [1] Smith, R. F., Eggert, J. H., Rudd, R. E., Swift, D. C., Bolme, C. A., and Collins, G. W., 2011, "High Strain-Rate Plastic Flow in Al and Fe," *J. Appl. Phys.*, **110**(12), p. 123515.
- [2] Cereceda, D., Diehl, M., Roters, F., Raabe, D., Perlado, J. M., and Marian, J., 2016, "Unraveling the Temperature Dependence of the Yield Strength in Single-Crystal Tungsten Using Atomistically-Informed Crystal Plasticity Calculations," *Int. J. Plast.*, **78**, pp. 242–265.
- [3] Gurrutxaga-Lerma, B., Shehadeh, M. A., Balint, D. S., Dini, D., Chen, L., and Eakins, D. E., 2017, "The Effect of Temperature on the Elastic Precursor Decay in Shock Loaded FCC Aluminium and BCC Iron," *Int. J. Plast.*, **96**, pp. 135–155.
- [4] Zaretsky, E. B., and Kanel, G. I., 2014, "Tantalum and Vanadium Response to Shock-Wave Loading at Normal and Elevated Temperatures. Non-Monotonous Decay of the Elastic Wave in Vanadium," *J. Appl. Phys.*, **115**(24), p. 243502.
- [5] Smith, R. F., Eggert, J. H., Jankowski, A., Celliers, P. M., Edwards, M. J., Gupta, Y. M., Asay, J. R., and Collins, G. W., 2007, "Stiff Response of Aluminum Under Ultrafast Shockless Compression to 110 GPa," *Phys. Rev. Lett.*, **98**(6), p. 065701.
- [6] Armstrong, R. W., Arnold, W., and Zerilli, F. J., 2007, "Dislocation Mechanics of Shock-Induced Plasticity," *Metall. Mater. Trans. A*, **38**(11), pp. 2605–2610.
- [7] Armstrong, R. W., and Zerilli, F. J., 2010, "High Rate Straining of Tantalum and Copper," *J. Phys. D: Appl. Phys.*, **43**(49), p. 492002.
- [8] Armstrong, R. W., and Li, Q., 2015, "Dislocation Mechanics of High-Rate Deformations," *Metall. Mater. Trans. A*, **46**(10), pp. 4438–4453.
- [9] Eggert, J. H., Smith, R. F., Swift, D. C., Rudd, R. E., Fratanduono, D. E., Braun, D. G., Hawrelak, J. A., McNaney, J. M., and Collins, G. W., 2015, "Ramp Compression of Tantalum to 330 GPa," *High Pressure Res.*, **35**(4), pp. 339–354.
- [10] Asay, J. R., Ao, T., Vogler, T. J., Davis, J. P., and Gray, G. T., 2009, "Yield Strength of Tantalum for Shockless Compression to 18 GPa," *J. Appl. Phys.*, **106**(7), p. 073515.
- [11] Zepeda-Ruiz, L. A., Stukowski, A., Oettel, T., and Bulatov, V. V., 2017, "Probing the Limits of Metal Plasticity With Molecular Dynamics Simulations," *Nature*, **550**(7677), pp. 492–495.
- [12] Armstrong, R. W., Arnold, W., and Zerilli, F. J., 2009, "Dislocation Mechanics of Copper and Iron in High Rate Deformation Tests," *J. Appl. Phys.*, **105**(2), p. 023511.
- [13] Orowan, E., 1940, "Problems of Plastic Gliding," *Proc. Phys. Soc.*, **52**(1), pp. 8–22.
- [14] Zerilli, F. J., and Armstrong, R. W., 1987, "Dislocation-Mechanics-Based Constitutive Relations for Material Dynamics Calculations," *J. Appl. Phys.*, **5**(5), pp. 1816–1825.
- [15] Zerilli, F. J., and Armstrong, R. W., 1990, "Description of Tantalum Deformation Behavior by Dislocation Mechanics Based Constitutive Relations," *J. Appl. Phys.*, **68**(4), pp. 1580–1591.
- [16] Lea, L., Brown, L., and Jardine, A., 2020, "Time Limited Self-Organised Criticality in the High Rate Deformation of Face Centred Cubic Metals," *Commun. Mater.*, **1**(1), pp. 1–8.
- [17] Swegle, J. W., and Grady, D. E., 1985, "Shock Viscosity and the Prediction of Shock Wave Rise Times," *J. Appl. Phys.*, **58**(2), pp. 692–701.
- [18] Zerilli, F. J., and Armstrong, R. W., 1992, "The Effect of Dislocation Drag on the Stress-Strain Behavior of FCC Metals," *Acta Metall. Mater.*, **40**(8), pp. 1803–1808.
- [19] El Ters, P., and Shehadeh, M. A., 2019, "Modeling the Temperature and High Strain Rate Sensitivity in BCC Iron: Atomistically Informed Multiscale Dislocation Dynamics Simulations," *Int. J. Plast.*, **112**, pp. 257–277.
- [20] Zbib, H. M., and Diaz de la Rubia, T., 2002, "A Multiscale Model of Plasticity," *Int. J. Plast.*, **18**(9), pp. 1133–1163.

- [21] Yasin, H., Zbib, H. M., and Khaleel, M. A., 2001, "Size and Boundary Effects in Discrete Dislocation Dynamics: Coupling With Continuum Finite Element," *Mater. Sci. Eng. A*, **309**, pp. 294–299.
- [22] Kattoura, M., and Shehadeh, M. A., 2014, "On the Ultra-High-Strain Rate Shock Deformation in Copper Single Crystals: Multiscale Dislocation Dynamics Simulations," *Philos. Mag. Lett.*, **94**(7), pp. 415–423.
- [23] Gillis, P. P., Gilman, J. J., and Taylor, J. W., 1969, "Stress Dependences of Dislocation Velocities," *Philos. Mag.*, **20**(164), pp. 279–289.
- [24] Gurrutxaga-Lerma, B., 2016, "The Role of the Mobility Law of Dislocations in the Plastic Response of Shock Loaded Pure Metals," *Modell. Simul. Mater. Sci. Eng.*, **24**(6), p. 065006.
- [25] Zbib, H. M., Hiratani, M., and Shehadeh, M. A., 2005, "Multiscale Discrete Dislocation Dynamics Plasticity," *Continuum Scale Simulation of Engineering Materials: Fundamentals-Microstructures-Process Applications*, pp. 201–229.
- [26] Bhate, N., Clifton, R. J., Kumar, S., and Phillips, R., 2002, "Computational and Experimental Studies of Dislocation Dynamics," *Shock Compression in Condensed Matter-2001: Proceeding of the Conference of the American Physical Society Topical Group on Shock Compression of Condensed Matter*, M. D. Furnish, N. N. Thadani, and Y. Hori, eds., American Institute of Physics, New York.
- [27] Hirth, J. P., Zbib, H. M., and Lothe, J., 1998, "Forces on High Velocity Dislocations," *Modell. Simul. Mater. Sci. Eng.*, **6**(2), pp. 165–169.
- [28] Leibfried, G., 1950, "Über den Einfluß thermisch Angeregter Schallwellen auf die Plastische Deformation," *Z. Phys.*, **127**(4), pp. 344–356.
- [29] Olmsted, D. L., Hector, L. G., Curtin, W. A., and Clifton, R. J., 2005, "Atomistic Simulations of Dislocation Mobility in Al, Ni and Al/Mg Alloys," *Modell. Simul. Mater. Sci. Eng.*, **13**(3), p. 371–388.
- [30] Firdu, F. T., and Taskinen, P., 2010, "Densities of Molten and Solid Alloys of (Fe, Cu, Ni, Co)—S at Elevated Temperatures—Literature Review and Analysis," Aalto University Publications in Materials Science and Engineering, Multiprint Oy, Espoo.
- [31] Tarumi, R., Shiraiishi, K., and Hirao, M., 2009, "High Temperature Elastic Constants of  $\alpha$ -Fe Single Crystal Studied by Electromagnetic Acoustic Resonance," *ISIJ Int.*, **49**(9), pp. 1432–1435.
- [32] Sha, X., and Cohen, R. E., 2006, "First-Principles Thermoelasticity of BCC Iron Under Pressure," *Phys. Rev. B*, **74**(21), p. 214111.
- [33] Wang, Z. Q., and Beyerlein, I. J., 2011, "An Atomistically-Informed Dislocation Dynamics Model for the Plastic Anisotropy and Tension-Compression Asymmetry of BCC Metals," *Int. J. Plast.*, **27**(10), pp. 1471–1484.
- [34] Gulseren, O., and Cohen, R. E., 2002, "High Pressure Thermoelasticity of Body-Centered Cubic Tantalum," *Phys. Rev. B*, **65**(6), p. 064103.
- [35] El Ters, P., and Shehadeh, M. A., 2020, "On the Strain Rate Sensitivity of Size-Dependent Plasticity in BCC Iron at Elevated Temperatures: Discrete Dislocation Dynamics Investigation," *Mech. Mater.*, **148**, p. 103494.
- [36] Shehadeh, M. A., 2012, "Multiscale Dislocation Dynamics Simulations of Shock-Induced Plasticity in Small Volumes," *Philos. Mag.*, **92**(10), pp. 1173–1197.
- [37] Shehadeh, M. A., Bringa, E. M., Zbib, H. M., McNaney, J. M., and Remington, B. A., 2006, "Simulation of Shock-Induced Plasticity Including Homogeneous and Heterogeneous Dislocation Nucleations," *Appl. Phys. Lett.*, **89**(17), p. 171918.
- [38] Shehadeh, M. A., Zbib, H. M., and De La Rubia, T. D., 2005, "Multiscale Dislocation Dynamics Simulations of Shock Compression in Copper Single Crystal," *Int. J. Plast.*, **21**(12), pp. 2369–2390.
- [39] Shehadeh, M. A., and Zbib, H. M., 2016, "On the Homogeneous Nucleation and Propagation of Dislocations Under Shock Compression," *Philos. Mag.*, **96**(26), pp. 2752–2778.
- [40] Shehadeh, M. A., 2011, "Modeling Shock Induced Plasticity in Copper Single Crystal: Numerical and Strain Localization Issues," *Adv. Mater. Res.*, **324**, pp. 193–196.
- [41] Hammel, B., Swift, D., El-Dasher, B., Kumar, M., Collins, G. W., and Florando, J., 2012, "Plastic Behavior of Polycrystalline Tantalum in the  $5 \times 10^7/s$  Regime," *AIP Conf. Proc.*, **1426**(1), pp. 931–934.
- [42] Arnold, W., 1992, "Dynamisches Werkstoffverhalten von Armco-Eisen bei Stoßwellenbelastung (Only in German Available), "Dynamical Material Behavior of Armco-Iron Under Shock Wave Loading", Ph.D. thesis, VDI-Verlag, Duesseldorf.
- [43] Evans, A. G., and Rawlings, R. D., 1969, "The Thermally Activated Deformation of Crystalline Materials," *Phys. Status Solidi B*, **34**(1), pp. 9–31.
- [44] Zhu, T., and Li, J., 2010, "Ultra-Strength Materials," *Prog. Mater. Sci.*, **55**(7), pp. 710–757.
- [45] Armstrong, R. W., 1973, "Thermal Activation Strain Rate Analysis (TASRA) for Polycrystalline Metals," *JSIR*, **32**.
- [46] Queyreau, S., Marian, J., Gilbert, M. R., and Wirth, B. D., 2011, "Edge Dislocation Mobilities in BCC Fe Obtained by Molecular Dynamics," *Phys. Rev. B*, **84**(6), p. 064106.
- [47] Rudd, R. E., Comley, A. J., Hawreliak, J., Maddox, B., Park, H. S., and Remington, B. A., 2012, "Theory and Simulation of 1D TO 3D Plastic Relaxation in Tantalum," *AIP Conf. Proc.*, **1426**(1), pp. 1379–1382.
- [48] Tramontina, D., Erhart, P., Germann, T., Hawreliak, J., Higginbotham, A., Park, N., Ravelo, R., Stukowski, A., Suggit, M., Tang, Y., Wark, J., and Bringa, E., 2014, "Molecular Dynamics Simulations of Shock-Induced Plasticity in Tantalum," *High Energy Density Phys.*, **10**, pp. 9–15.